Cell Cycle 14:18, 2969–2984; September 15, 2015; Published with license by Taylor & Francis Group, LLC

Role of stress-activated OCT4A in the cell fate decisions of embryonal carcinoma cells treated with etoposide

Anda Huna[1], Kristine Salmina[1], Jekaterina Erenpreisa[1], Alejandro Vazquez-Martin[1], Jekabs Krigerts[1], Inna Inashkina[1], Bogdan I Gerashchenko[1,4], Paul A Townsend[2], Mark S Cragg[3], and Thomas R Jackson[2,*]

[1]Latvian Biomedical Research and Study Center; Riga, Latvia; [2]Institute of Cancer Sciences; Manchester Cancer Research Center; University of Manchester; Manchester Academic Health Science Center; Manchester, UK; [3]Cancer Sciences Unit; University of Southampton; Faculty of Medicine; General Hospital; Southampton, UK; [4]R. E. Kavetsky Institute of Experimental Pathology; Oncology and Radiobiology; National Academy of Sciences of Ukraine; Kyiv, Ukraine

Keywords: cell-fate, DNA damage, OCT4A/POU5F1, p53, p21Cip1, p16ink4a, p62, pluripotency, senescence, self-renewal, tumor cells

Abbreviations: AMPK, AMP-activated protein kinase; Baf, bafilomycin; EC, embryonal carcinoma; ES, embryonic stem; ETO, Etoposide; IF, immunofluorescent; LC3, microtubule associated protein 1 light chain 3; NT, non-treated; NT2, NTera 2; ntg, non-target; pCHK2, phosphorylated CHK2; PI, propidium iodide; siRNA, small interfering RNA; shRNA, small hairpin RNA; Sa-b-gal, senescence associated β-galactosidase.

Tumor cellular senescence induced by genotoxic treatments has recently been found to be paradoxically linked to the induction of "stemness." This observation is critical as it directly impinges upon the response of tumors to current chemo-radio-therapy treatment regimens. Previously, we showed that following etoposide (ETO) treatment embryonal carcinoma PA-1 cells undergo a p53-dependent upregulation of OCT4A and p21Cip1 (governing self-renewal and regulating cell cycle inhibition and senescence, respectively). Here we report further detail on the relationship between these and other critical cell-fate regulators. PA-1 cells treated with ETO display highly heterogeneous increases in OCT4A and p21Cip1 indicative of dis-adaptation catastrophe. Silencing OCT4A suppresses p21Cip1, changes cell cycle regulation and subsequently suppresses terminal senescence; p21Cip1-silencing did not affect OCT4A expression or cellular phenotype. SOX2 and NANOG expression did not change following ETO treatment suggesting a dissociation of OCT4A from its pluripotency function. Instead, ETO-induced OCT4A was concomitant with activation of AMPK, a key component of metabolic stress and autophagy regulation. p16ink4a, the inducer of terminal senescence, underwent autophagic sequestration in the cytoplasm of ETO-treated cells, allowing alternative cell fates. Accordingly, failure of autophagy was accompanied by an accumulation of p16ink4a, nuclear disintegration, and loss of cell recovery. Together, these findings imply that OCT4A induction following DNA damage in PA-1 cells, performs a cell stress, rather than self-renewal, function by moderating the expression of p21Cip1, which alongside AMPK helps to then regulate autophagy. Moreover, this data indicates that exhaustion of autophagy, through persistent DNA damage, is the cause of terminal cellular senescence.

Introduction

The relationship between cancer cells, normal stem cells, and cancer stem cells represents a question of substantial current interest.[1] It has been proposed that transcription networks that confer stem cell properties such as self-renewal, plasticity, or an increased resistance to genotoxic stimuli in normal stem cells may perform a similar function in cancer cells.[2] This hypothesis is supported by the growing clinical evidence that expression of key embryonal stem cell (ESC) transcription factors POU1F5 (OCT4A), NANOG and SOX2, are associated with poorer prognosis through tumor resistance, recurrence and progression in a wide variety of cancers.[3-9] Furthermore, it has been demonstrated by several groups that ESC transcription factors can be upregulated in response to DNA damage where they likely play a role in regulating survival.[10-12]

Conversely, accelerated cellular senescence is a phenomenon that has also been shown to be induced by genotoxic treatments of cancer cells.[13] Cellular senescence has traditionally been considered a terminal cell fate.[13,14] However, more recently it has been shown to be reversible at early stages, at least in tumor cells.[15-18] Furthermore, a direct link between senescence and

*Correspondence to: Thomas Robert Jackson; Email: tom.jackson-2@manchester.ac.uk

Submitted: 04/17/2015; Revised: 05/22/2015; Accepted: 05/27/2015

http://dx.doi.org/10.1080/15384101.2015.1056948

"stemness," essential cytological characteristics of a stem cell that distinguishes it from ordinary somatic cells, emerged in experiments where pluripotency is induced in normal cells.[19,20]

The molecular regulators of these processes in normal embryonal development, such as p21Cip1, are slowly becoming discerned.[21] One intriguing observation is that embryonal cellular senescence is associated with upregulation of the same pathways which govern the epithelial-mesenchymal transition (EMT).[22] This, apparently paradoxical, link between opposites in cell fate provides a challenge for scientific reasoning.

We have previously observed in IMR90 fibroblasts that a pre-senescent phenotype is associated with the appearance of self-renewal and senescence markers coupled to DNA damage.[23] We also demonstrated co-incident p53-dependent upregulation of 2 opposing cell fate regulators, p21Cip1 and OCT4A in embryonal carcinoma PA-1 cells treated with Etoposide (ETO).[24] We hypothesized that this bi-potential state favors DNA damage repair (DDR) while preventing full commitment to either senescence or self-renewal. In this system, p53 silencing promoted terminal senescence and premature mitosis. Together these data support the presence of a pre-senescent cell state which can arise in response to both senescence and stemness programmes being coactivated in response to genotoxic damage.

In the present study, we asked how key regulators of stemness (OCT4A, SOX2 and NANOG) and senescence (p16inka4a) behave in individual PA-1 cells during the response of ETO-induced DNA damage. Using siRNA silencing approaches we addressed the effect of OCT4A and p21Cip1 expression on each other and subsequent cell fates, determining the role of autophagy and how OCT4A activation impacts on the energy and genomic stress sensor and master metabolic regulator and activator of autophagy AMP-activated protein kinase (AMPK).

Results

Etoposide-treatment elicits a senescence-like phenotype in PA-1 cells

Following ETO treatment many PA-1 cells undergo gradual cell apoptosis and anoikis, while the remainder arrest in G2M and upregulate p53 and p21Cip.[24] G2M arrest and nuclear swelling were evident on day 3 after ETO treatment, with restoration of normal cell cycle and nuclear size 4 d later (**Fig. 1A and B**). Concurrent nuclear area assessments and DNA content measurements demonstrate that the nuclei of ETO treated cells increased in size irrespective of the stage of the cell cycle, but was most evident in G2M and polyploid cells (**Fig. 1C and D**). Increased nuclear area and DNA content were also accompanied by an increase in cellular granularity, as determined by an increase in side scatter detected by flow cytometry analysis (**Fig. 1E**), and autophagy (see below). The majority of cells displayed flattened morphology (**Fig. 1F**), but only a proportion displayed p16Ink4a nuclear positivity (**Fig. 1 G, H**). Furthermore, p16Ink4a expression was largely confined to the cytoplasm (**Fig. 1 G**). All of these features are indicative of senescence.

Heterogeneous expression of OCT4A and p21Cip1 following Etoposide treatment

We previously showed that the senescence marker p21Cip1 and the stemness marker OCT4A simultaneously increase and co-exist in the same cells following ETO treatment.[24] After confirming the pre-senescent phenotype of these cells, we next wished to explore how these critical factors for cell fate were dynamically regulated, integrated and diversified. As judged by flow cytometry ~60% of the cells become positive for both markers at the peak of the response (day 5), thereafter the expression of both markers and the proportion of double positive cells gradually decreases (**Fig. 2A**) as clonogenic, mitotic division ensues. To exclude the possible impact of the senescence-associated cytoplasmic and nuclear area changes on the flow cytometry measurements, semi-automatic image cytometry was undertaken, measuring the expression of both factors in the cell nucleus (apoptotic cells possessing very high p21Cip1 positivity lacking OCT4A were deliberately excluded from this analysis as distorting stoichiometry of measurements). Both the expression and variation of expression of OCT4A and p21Cip1 increased on day 3 after ETO treatment; and increased further on day 5 (**Fig2B and C**, **Fig. S1**) and a high number of double-positive cells confirmed (**Fig. 2B**).

OCT4A upregulation is not accompanied by changes in SOX2 or NANOG

In its function as a master regulator of pluripotency and self-renewal, OCT4A cooperates with SOX2 and NANOG whose expression are therefore required for maintaining the embryonic stem cell phenotype.[25] We thus explored the expression of these transcription factors in the DNA damage response of PA-1 cells. Immunoblotting confirmed that p53 increased in response to ETO from day 1, resulting in the induction of p21Cip1, which reached its maximum on day 5 (**Fig 3A**). As documented previously, OCT4A expression was present in control cells and increased following ETO treatment, coincident with p53 upregulation.[24] Weak expression of SOX2 was found in untreated cells but did not alter following ETO-treatment (**Fig. 3A**); a result confirmed by image cytometry measurements in individual cells (**Fig3B**, **Fig. S1**). NANOG was not detected in PA-1 cells by immunoblotting (**Fig 3A**) although rare NANOG positive cells (less than 5%) were found in control and ETO-treated samples by 3 different antibodies (Supplementary **Fig. 1**). Intriguingly, SOX2 failed to show unambiguous antagonism with p21Cip1, which has previously been reported as directly inhibiting SOX2 in neurodifferentiation.[26] Furthermore, SOX2 expression did not show significant correlation with its self-renewal partner OCT4A (data not shown). Together, these data suggest a dissociation of OCT4A from its self-renewal capacity when it is induced by p53 (in the presence of p21Cip1) in response to DNA damage.

OCT4A suppresses p21Cip1 and promotes an enhanced senescence phenotype

Given its potential lack of self-renewal capacity, we next investigated the role of OCT4A in PA-1 cells following ETO

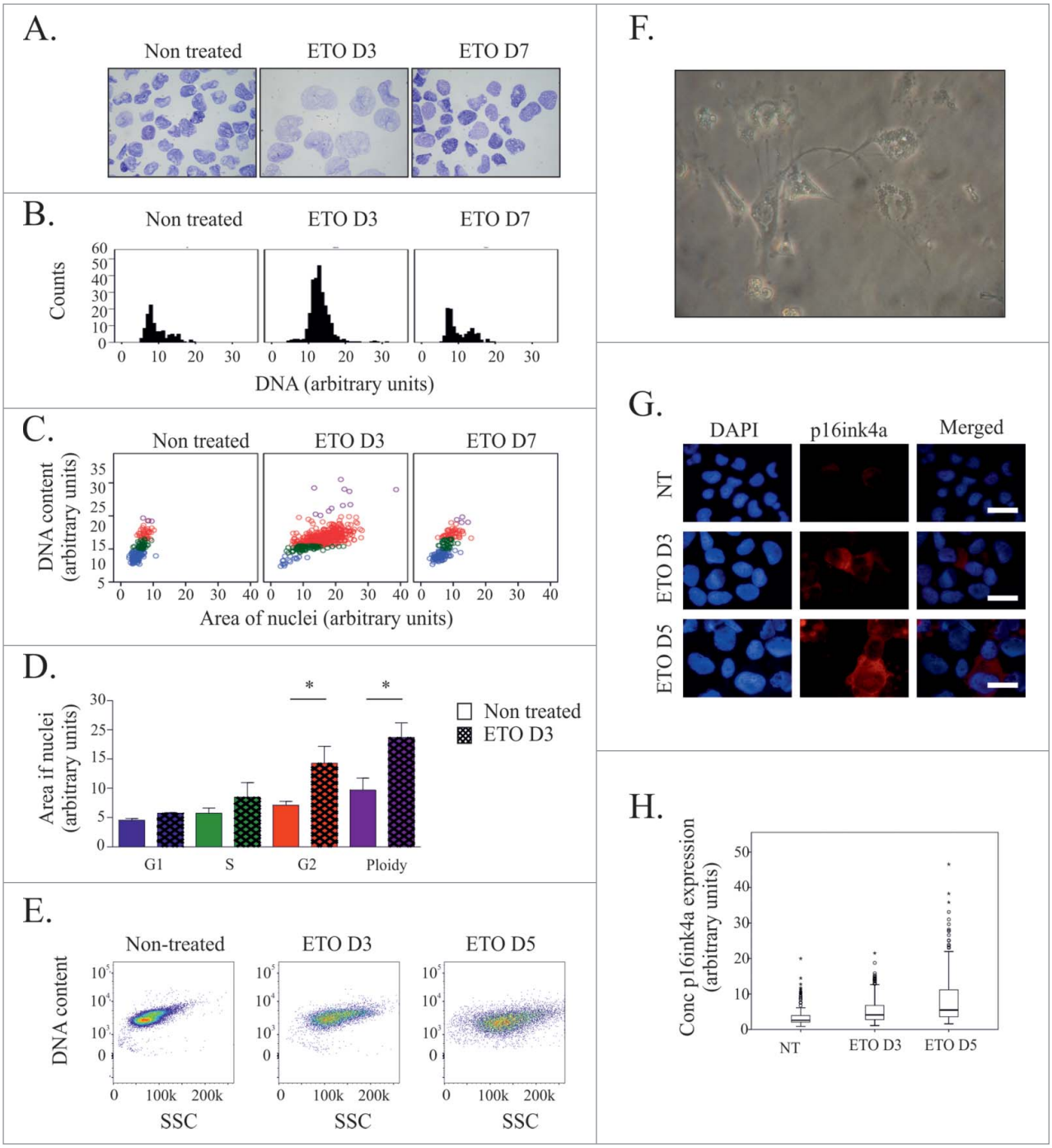

Figure 1. Senescent-like phenotype of ETO-treated PA-1 cells. PA-1 cells were treated with 8 μM ETO for 20 h before being replaced with fresh media. (**A-D**) DNA content and nuclear area were assessed using toluidine blue staining at indicated time points. (**A**) Images of toluidine blue stained nuclei at indicated time points. (**B**) Histograms of DNA content were produced and used to determine the cell cycle stage of individual cells. (**C**) Dot-plots of DNA content versus nuclei area with each cell colored according to cell cycle stage as determined by DNA content histograms: G1 (blue); S phase (green); G2 (red); purple (polyploid). A statistically significant difference in nuclear size between treated and non-treated cells was observed in G2 and polyploid fractions (*$p < 0.05$, $n = 3$). (**E**) Granularity of cells (SSC) was measured at indicated time points by flow cytometry. (**F**) Phase contrast microscopy of PA-1 cells displaying a flattened morphology. (**G**) Immunofluorescence staining for p16ink4a (red) and counterstained with DAPI at indicated time points demonstrating an increase in p16ink4a following ETO treatment. (**H**) Quantification of p16ink4a expression determined in individual cells by image cytometry displayed as a box plot showing its increase after ETO treatment. Images are representative for at least 3 individual experiments.

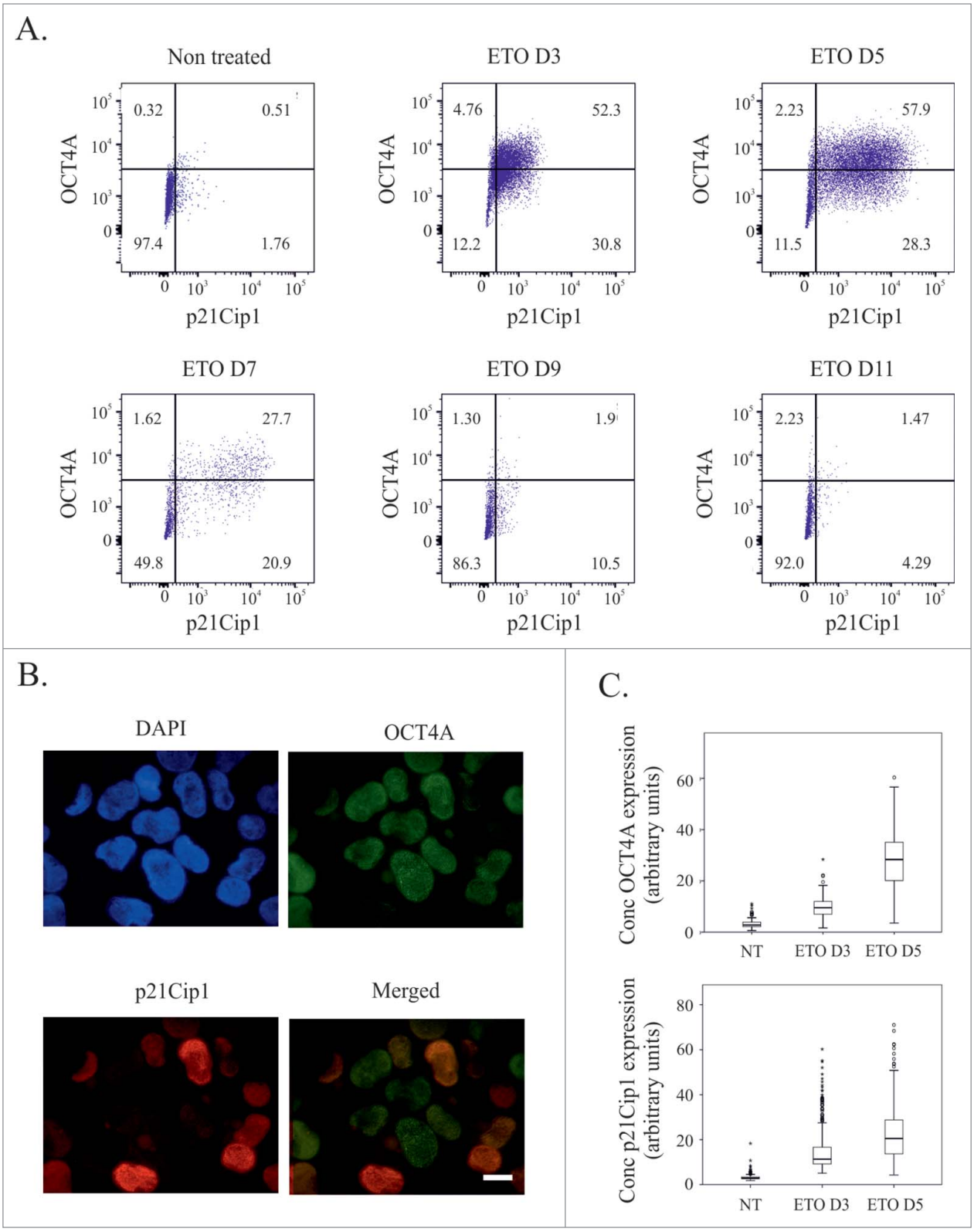

Figure 2. Expression of OCT4A and p21Cip1 following ETO treatment of PA-1 cells. (**A**) Dual staining for OCT4A and p21cip1 by immunofluorescence 3 d after ETO treatment. (**B**) Quantitation of OCT4A and p21Cip1 expression on day 3 and day 5 after ETO treatment as measured by image cytometry. (**C**) Detection of OCT4A and p21Cip1 by flow cytometry after ETO treatment. Data collected over 11 d indicate an increasing expression and heterogeneity, with numerous double positive cells at the time of maximal increase (day 5). Starting from day 7 their expression, double-positive population and degree of heterogeneity gradually decreases during the recovery of clonogenic growth.

treatment using siRNA. Prior to this analysis, we first established which OCT4 isoforms were expressed in PA-1 cells. Using a panel of specific mAb, immunoblotting revealed that OCT4B was undetectable in these cells both before and after ETO treatment (**Fig. S2**), consistent with published previously RT-PCR data.[24]

Having established that OCT4B was not expressed in PA-1 cells, siRNA silencing was used to assess the role of OCT4A in their response to ETO treatment. Efficient (80–95%) knock-down of OCT4A was confirmed with 3 different siRNA, in addition to a 3 siRNA pool (**Fig. S3**) and the molecular response to ETO was then examined by immunoblotting (**Fig 4A**) for key regulators of DNA damage, (pCHK2, p53, p21Cip1, and RAD51). These experiments revealed p53, RAD51 and pCHK2 were all upregulated from day 1 independently of OCT4A expression. p21Cip1 expression rose gradually from day 1 throughout the course of experiment as seen in previous experiments. Silencing of OCT4A resulted in a marked increase in p21Cip1 expression from day 1. These results imply that the presence of OCT4A induced by DNA damage suppresses p21Cip1 expression despite comparable levels of p53 expression and equivalent DNA damage as judged by RAD51 and pCHK2 expression.

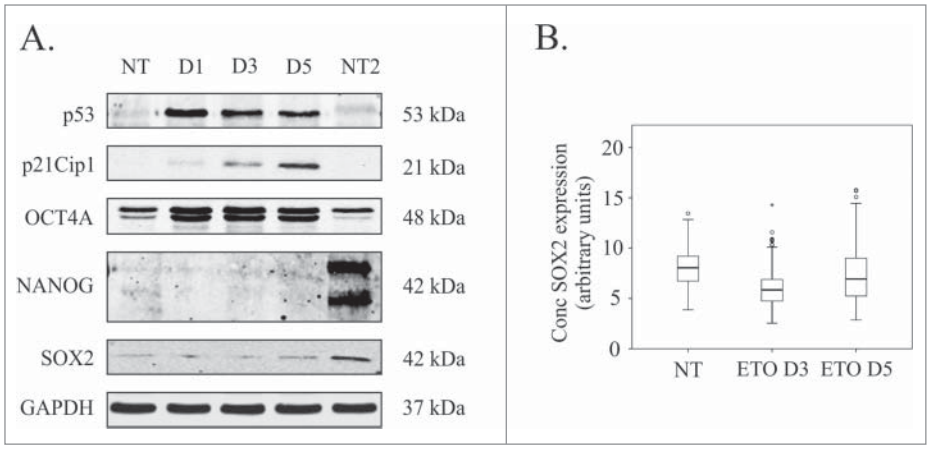

Figure 3. Analysis of pluripotency transcription factors in response to ETO treatment in PA-1 cells. (**A**) Protein expression of p53, p21Cip1, OCT4A, SOX2 and NANOG were analyzed by immunoblotting at indicated time points after ETO-treatment. GAPDH was used as a loading control NT2 cells were used as a positive control for pluripotency genes OCT4A, SOX2 and NANOG. p53 and p2Cip1 protein expression was upregulated in the DNA damage response. An upregulation of the OCT4A protein was detected from day 1 post ETO treatment, while SOX2 remained low and unchanged post ETO expression. NANOG was not detected in NT or ETO treated PA-1 cells. Results are representative of 3 independent experiments. (**B**) Semi-automatic image cytometry of SOX2 expression was performed on the nuclei of individual cells. Box-plots indicate the heterogeneity and expression levels measured. The data show that SOX2 remains unresponsive to ETO-treatment.

When investigating the cell cycle response, loss of OCT4A caused an almost identical phenotype to that previously reported with p53 silencing[24] i.e. OCT4A-silenced cells underwent a profound G2M arrest with apoptosis being greatly reduced (**Fig. 4B and C**). The cells displayed the large, flattened morphology and Sa-β-gal staining associated with senescence on day 5 (**Fig. 4D**), identical to that previously reported when silencing p53. Thus, the increase in G2M arrest and increased accelerated senescence previously observed with p53 silencing appears to be entirely due to the loss of the induction of OCT4A. Prolonged loss of OCT4A lead to the polyploidisation of these senescent cells and a reduction in clonal recovery (**Fig. 5**). The absence of off target effects was confirmed by repeating silencing and cell cycle analysis experiments with 3 separate siRNA molecules targeting different sequences of OCT4A mRNA (Supplementary **Fig. 4**).

p21Cip1 silencing does not affect OCT4A expression or cell cycle arrest

Having established that OCT4A suppresses p21Cip1 and a senescent phenotype we sought to investigate the possibility of a reciprocal suppression of OCT4A by p21Cip1. To do this p21Cip1 was silenced using siRNA. Silencing of p21Cip1 was efficient as judged by immunoblotting but was not found to affect the expression of OCT4A in the presence or absence of ETO treatment (**Fig. 6**). Furthermore, we detected no difference in the cell cycle profiles of p21Cip1-silenced cells compared to control siRNA treated cells following ETO treatment.

In summary, we found that OCT4A tempers p21Cip1 upregulation, restricting entry into senescence, indicating that co-expression defines the pre-senescent state. While p21Cip1 did not regulate OCT4A expression or change the cell cycle, depletion of OCT4A profoundly impacted it. We also found that p53-activated OCT4A does not support the pluripotency network in pre-senescent cells (owing to the lack of SOX2/NANOG co-ordination), leaving its biological role unclear. We, therefore, interrogated its possible role as a stress responder where one of these stresses may be metabolic. AMPK is a key sensor of metabolism and energy status.[27] Therefore, we next explored the activation of AMPK by virtue of its phosphorylation at Threonine 172 ($pAMPK^{Thr172}$), in relation to OCT4A expression.

AMPK and OCT4A are coordinately activated in response to ETO-treatment

The results of this comparative study are shown in **Fig. 7**. Microscopy of control, untreated, cells revealed heterogeneous $pAMPK^{Thr172}$ activation with expression in some cell nuclei and also in centrosomes, central spindle and mid-bodies of mitotic cells as described previously,[28] and rarely (<1% cells), in the cytoplasm (**Fig. 7A**, upper row). In ETO-treated cells the staining for AMPK increased and strikingly coincided with the localization and intensity of staining for OCT4A in most cells (**Fig. 7A**, second row) as also confirmed by IF measurements, where clear correlation was shown (**Fig. 7B**). However, while OCT4A is seen homogenously throughout the nucleus

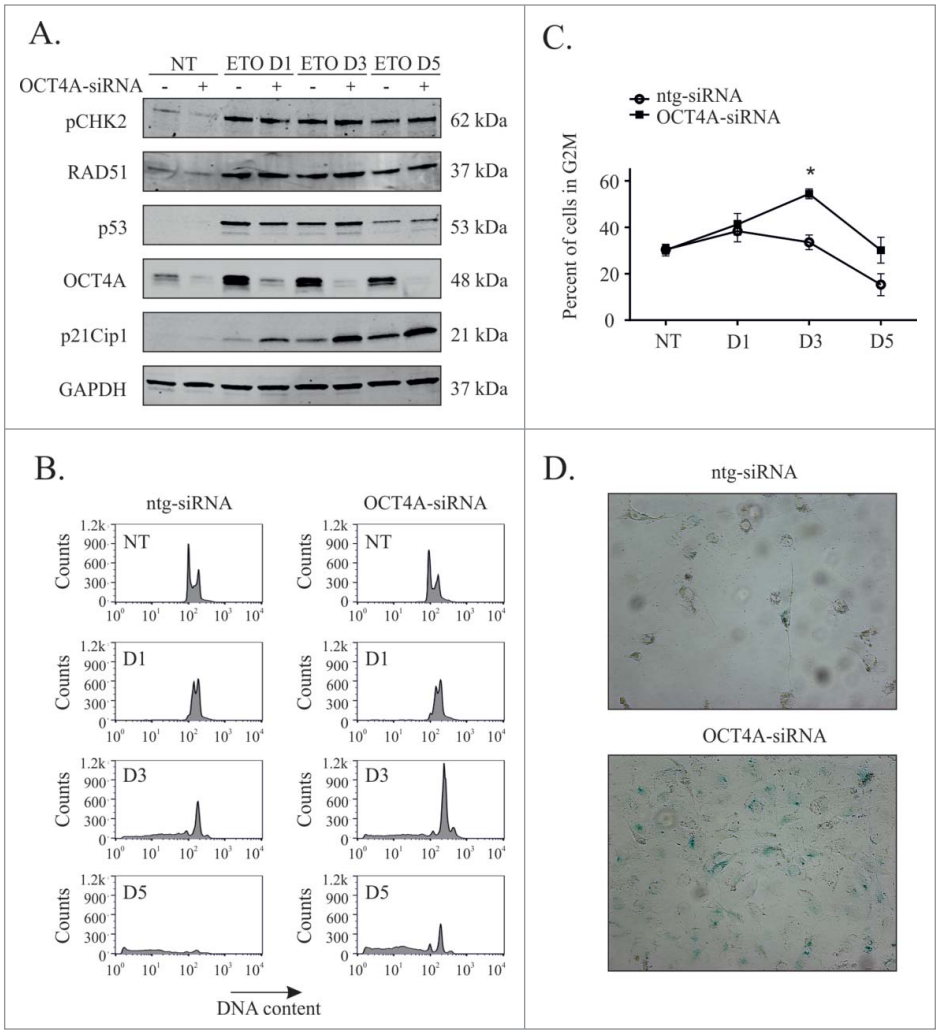

Figure 4. OCT4A suppresses p21, G2 arrest and induces senescence. PA-1 cells were treated with ntg-siRNA or OCT4-siRNA for 24 h before treatment with 8 μM ETO for 20 h and replacement with fresh media. (**A**) Protein expression was assessed at the indicated time points by immunoblotting. Cell lysates were made and assessed by immunoblotting for pCHK2, RAD51, p53, p21Cip1, OCT4A and GAPDH as a loading control. (**B**) Cells were fixed, stained with PtdIns and analyzed by flow cytometry. Both ntg-siRNA treated and OCT4-siRNA treated cells underwent a G2M arrest followibg ETO treatment, which is more profound at day 3 and 5 in OCT4A-siRNA-treated cells. There is subsequently a much lower extent of cell death (sub G1) in OCT4A-siRNA treated cells. (**C**) The G2M arrest was calculated from the DNA histograms shown in (**B**) and demonstrate significantly higher levels in OCT4A-silenced cells (*$p < 0.05$, $n = 3$). (**D**) PA-1 cells were treated with ETO as above and assessed for Sa-β-gal activity after 5 d Senescence, as monitored by Sa-β-gal activity, was increased by OCT4A-silencing. Both ntg-siRNA and OCT4A-siRNA treated cells became large following ETO treatment but non-silenced cells lacked Sa-β-gal activity.

pAMPK^{Thr172} staining revealed a fine (euchromatic) nuclear pattern, which indicates binding to chromatin, unlike OCT4A.

Intense staining of pAMPK^{Thr172} was also found in apoptotic cell nuclei and bodies, while OCT4A was not (**Fig. 7C**). In arrested metaphases appearing after ETO on day 4, pAMPK^{Thr172} was localized to multiple centrosomes, while OCT4A was not (**Fig. 7A**, second row). This difference in staining was confirmed by co-staining for γ-tubulin and AURORA B kinase (not shown). Together, these data indicate that OCT4A is co-ordinately regulated alongside pAMPK^{Thr172} in interphase cells but that in apoptotic cells their functions may differ. Moreover, the concordant expression of OCT4A and pAMPK^{Thr172} in interphase cells suggests that the p53-dependent OCT4A induction is a result of a stress response following ETO treatment.

As a part of its role as a central metabolic regulator, AMPK is directly involved in the regulation of autophagy.[29] In this regard, previous studies have shown that autophagy is implicated in the chemo-resistance to ETO and this effect is reversed by inhibition of AMPK, which led to cell death by apoptosis.[30]

Conversely, cellular senescence is also associated with autophagy[30] representing another potential cell fate phenotype following ETO-treatment.[24] p16ink4a is believed to drive irreversible senescence. [31] Therefore, we next decided to explore the relationship of p16ink4a and macroautophagy.

p16ink4a is sequestered by autophagy in ETO-treated cells

Autophagy was verified using immunofluorescence for p62 as a marker of autophagy. Post ETO treatment, an increase in the number of p62 foci/cell was observed by immunofluorescence (**Fig. 8A and B**) and mean number of p62 foci/cell in 3 independent experiments was shown to increase > 5-fold (**Fig 8C**). Bafilomycin A (Baf) halted autophagic flux in ETO-treated cells (shown as an accumulation of LC3B in relation to LC3A), confirming functional autophagy and its suppression (**Fig. 8D**). Baf treatment also enhanced cell death preventing clonogenic recovery only in ETO-treated cells (**Fig. S5**), which indicates the importance of autophagy for cell survival after DNA damage.

We then assessed immunostaining for p16ink4a and LAMP2 in the presence and absence of Baf post ETO treatment. LAMP2 is an important regulator of lysosomal biogenesis, required for the maturation of functional autophagosomes. In control, untreated cells, p16ink4a was observed in ~5% of cells as small aggresomes, surrounded by LAMP2-positive foci (data not shown). In ETO-treated cells (day 4), the cytoplasm was highly enriched with LAMP2, while p16ink4a-positive aggresomes (larger and more numerous than in control) were sequestered in

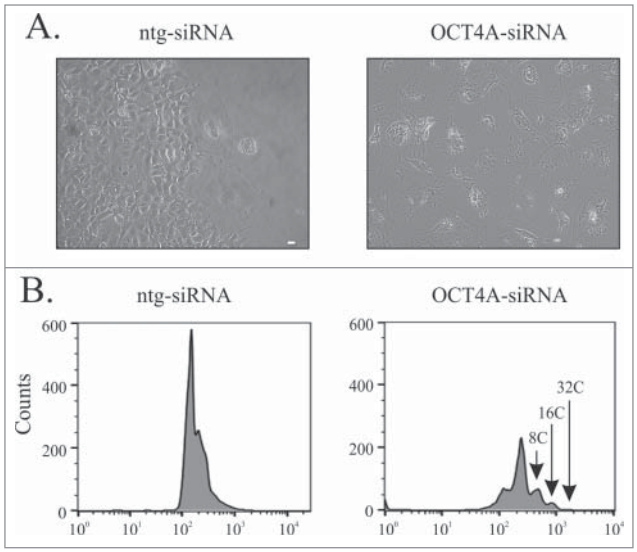

Figure 5. OCT4A silencing inhibits clonal recovery of ETO-treated PA-1 cells. PA-1 cells were treated with ntg-siRNA or OCT4A-siRNA for 24 h before treatment with 8 μM ETO for 20 h and replacement with fresh media. Cells were maintained until day 11. Clonal recovery was observed in non-silenced cells but not in OCT4A-silenced cells, which maintained a flat senescent like morphology. (**B**) Cells were fixed, stained with PI and analyzed by flow cytometry. A return of the G1 peak was observed in non-silenced ntg cells whereas OCT4A-silenced cells maintained a profound G2 arrest. OCT4A-silenced cells entered rounds of endoreduplication with genomes as large as 32C observed.

autophago-lysosomes (**Fig. 9 A and B**). Approximately 30% of cells were seen to accumulate large amounts of p16ink4a in multiple aggresomes, as measure by >3 aggresomes and/or diffusely detected within cytoplasm, or in large vacuoles (**Fig. 9A-C**), and often showed DNA in cytoplasm (**Fig. 9C**). The proportion of such cells, with high levels of p16ink4a, increased fold2- (29 ± 6 .5 and 58 ± 3 .5, +/− Baf, respectively) as measured on day 4. These observations indicate the important role of autophagy in sequestering and degrading p16ink4a in ETO-treated PA-1 cells, thus preventing senescence. They also show that a considerable proportion of ETO-treated cells suffer from exhaustion of autophagy.

Failure of autophagy to sequester p16ink4a in the cytoplasm is accompanied by drastic nuclear changes and loss of DNA

In ETO-treated samples counterstained with DAPI, we noted that the failure of macroautophagy to control and sequester p16ink4a in the cytoplasm coincided with prominent changes in cell nuclei, particularly following Baf treatment. Nuclei became thinner, less intensely DAPI-stained (e.g. **Fig. 9C**), or, more frequently, displaced to one of the cell poles by large autophagic vacuoles (**Fig. 9B**). Twisting, thinning, and disintegrating cell nuclei were the main phenotypes of ETO+Baf-treated cells. As detailed above, in their extreme distortions, the cell nuclei were displaced and squeezed by large autophagic vacuoles and attained a sickle-like shape (**Fig. 9D**). It remains possible that the loss of sequestration of p16ink4a, distortion of cell nuclei and loss of DNA are all linked, belonging to a related series of processes associated with exhausted autophagy, which is further exaggerated by Baf where full disintegration of the cell nucleus and alveolar LC3-positive cytoplasm are evident (**Fig. 10 A**).

Trying to understand how the penetrability of the cell nuclei was related to DNA damage we stained with an antibody (PL2–6) which detects a unique epitope involving a ternary complex of histones H2A and H2B and DNA at the site of the chromatin attachment to lamin B1.[32] We applied it to ETO-treated cell nuclei (day 4) combining it with a label for DNA damage (pCHK2). The result shows (**Fig. 10B**) bright nuclear staining with PL2–6 in cell nuclei without DNA damage and its reduction in cell nuclei containing DNA damage, possibly suggesting that binding to lamin B receptors in compromised.

In view of this data, we decided to use detailed stoichiometric DNA image cytometry following ETO treatment in the presence or absence of Baf. Typical histograms from one representative experiment are shown in **Fig. 10C**, while in **Fig. S6** comparative DNA histograms of selected normal- and sickle-shaped cell nuclei from ETO+Baf treatment are presented. Measurements from ETO-treated cells revealed a peak of delay in late S-phase, which was augmented after Baf treatment showing apparent redistribution from G2 (4C) into <4C, which was exaggerated in selected sickle-type nuclei of ETO+Baf-treated cells (**Fig. S6**). These data support our microscopic observations that DNA is preferentially lost from the sickle-like shape nuclei in the cells as a result of failed autophagic processing with the proportion of sickle-like nuclei cells with sickle-like nuclei in ETO-treated samples increased more than 2-fold (2.38 ± 0.2) following Baf treatment (n = 3).

Discussion

In this study, we expanded our investigation of the response of PA-1 embryonal carcinoma cells to DNA damaging chemotherapy. We previously observed,[24] a concurrent p53-dependent increase in OCT4A and p21Cip1 protein expression after ETO-treatment, with the resulting cells transiting through an apparently bi-potential state with hallmarks of both premature multicentriolar mitoses and senescence. Herein, we extended our analysis and highlight a hitherto unobserved DNA damage response (DDR) function of OCT4A following ETO treatment, which is different from its established pluripotency and self-renewal functions. This p53-dependant DDR-induced OCT4A is not coordinated with SOX2 or NANOG activity, but does serve to suppress p21Cip1. This finding is in accord with the previously shown observation that OCT4A can directly repress p21Cip1 expression by binding its promoter in the absence of SOX2 and NANOG. [33] Although not yet confirmed in other cell types or following different stimuli, this phenomenon likely relates to properties evidenced during embryonal 'stemness', as similar nuclear accumulation of OCT4A was similarly recently reported following laser beam damage of live ESC cells.[34]

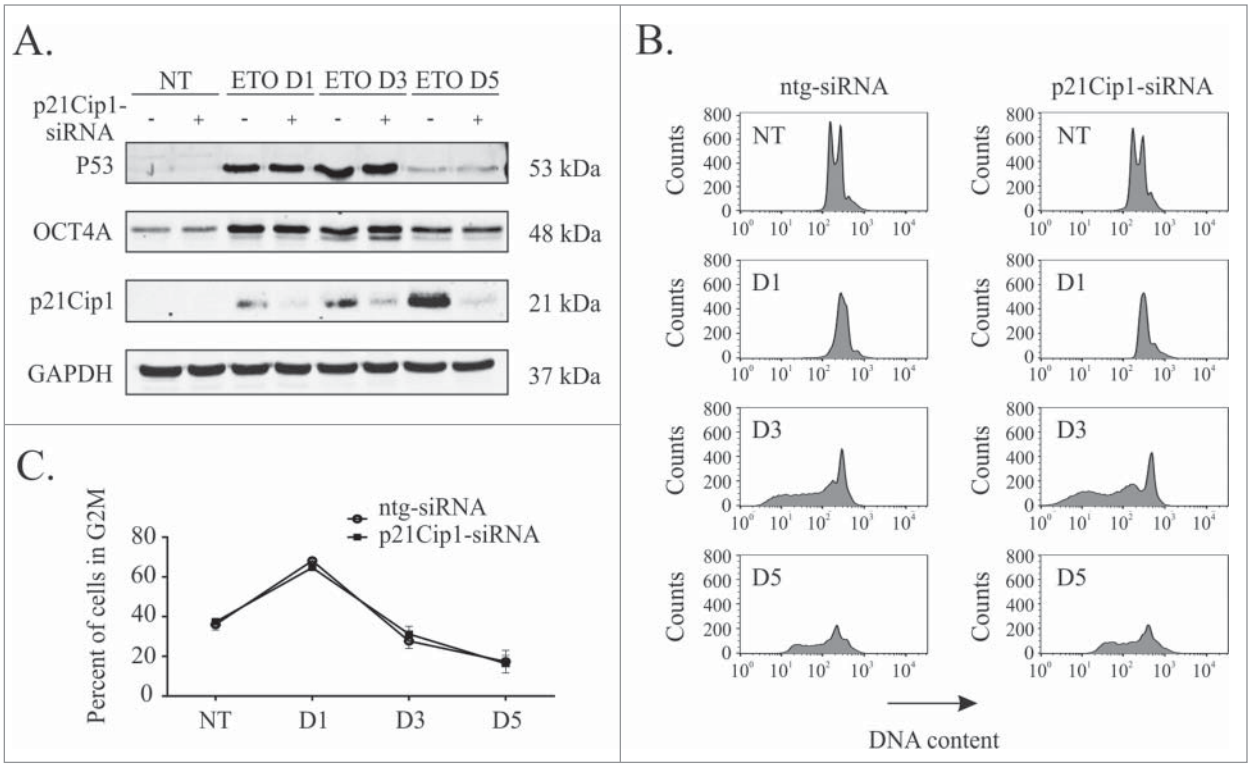

Figure 6. p21Cip1 expression does not affect G2M arrest in response to ETO treatment of PA-1 cells. PA-1 cells were treated with ntg-siRNA or p21Cip1-siRNA for 24 h before treatment with 8 μM ETO for 20 h and replacement with fresh media. (**A**) Expression of OCT4A, p21Cip1 and p53 were assessed at the indicated time points by immunoblotting. GAPDH was used as a loading control. (**B**) Cells were fixed, stained with PtdIns and analyzed by flow cytomtery. Both ntg-siRNA treated and p21Cip1-siRNA treated cells underwent a comparable G2M arrest after ETO treatment. (**C**) There was no significant difference in G2M arrest between p21Cip1 silenced and non-silenced cells.

Our measurements of OCT4A and p21Cip1 expression in individual cells revealed that cell fate, in response to extensive DNA damage, occurs with high levels of heterogeneity. Both factors increase coordinately with huge variations in expression, covering (at day 5) a wide spectrum of p21Cip1 and OCT4A expression.[35] These observations demonstrate a typical characteristic of self-organizing, adapting systems, using heterogeneity over time to provide bifurcations of cell fate choice.[36,37] The increased variance in both factors – from day 3 until day 7 – corresponds to the period with most prominent cell death (99% cells will die and only <1% has the chance to survive, likely representing the degree of challenge that they must overcome).[24] When OCT4A is silenced the level of p21Cip1 increases, more cells enter senescence and mitotic recovery is reduced, abrogating fragile balance in bifurcation point and removing the possibility for rare cells to choose survival as their fate. It is worth noting that this response was phenotypically identical to that seen when silencing p53.[24] We hypothesize that the loss of p53 or OCT4A in silencing experiments causes the loss of the embryonal G2M checkpoint leading to increased mitotic slippage, ultimately ending in terminal senescence rather than executing the G2M checkpoint function via apoptosis. Continued silencing of OCT4A inhibited clonogenic recovery post ETO treatment highlighting the importance of the pre-senescent G2M arrest for clonogenic recovery of the small percentage of cells that are able to repair their DNA damage. Silencing of OCT4A also leads to endoreplication in senescent cells further eluding to the presence of mitotic slippage.[38] p21Cip1 silencing experiments demonstrated that the observed G2M arrest was independent of p21Cip1 expression.

Mitotic survival of the ETO-treated cells ultimately originates from metastable pre-senescence. Theoretically, this means that the self-renewal function of OCT4A is finally restored. The attractor of self-renewal fate in individual cells is high NANOG,[39] released from direct suppression by p53[40] and activated by OCT4A-SOX2 heterodimer. Although NANOG is only found in a very small number of PA-1 cells, its role requires further exploration.

This moderator function of DDR-induced OCT4A occurs alongside activation of AMPK. AMPK is an evolutionary conserved low-energy checkpoint that operates as a master regulator of cellular metabolism and activator of autophagy. AMPK also acts as a genomic stress sensor that is required for the adaptation of metabolism switches and the DDR for efficient repair of DNA.[41] We previously observed a bidirectional relationship between AMPK and ATM/CHK2 pathways that integrates both the metabolic and DNA damage stress signaling.[42] AMPK activation was previously shown as necessary for maximal stress-induced transcription of p53-dependent genes that promote cell

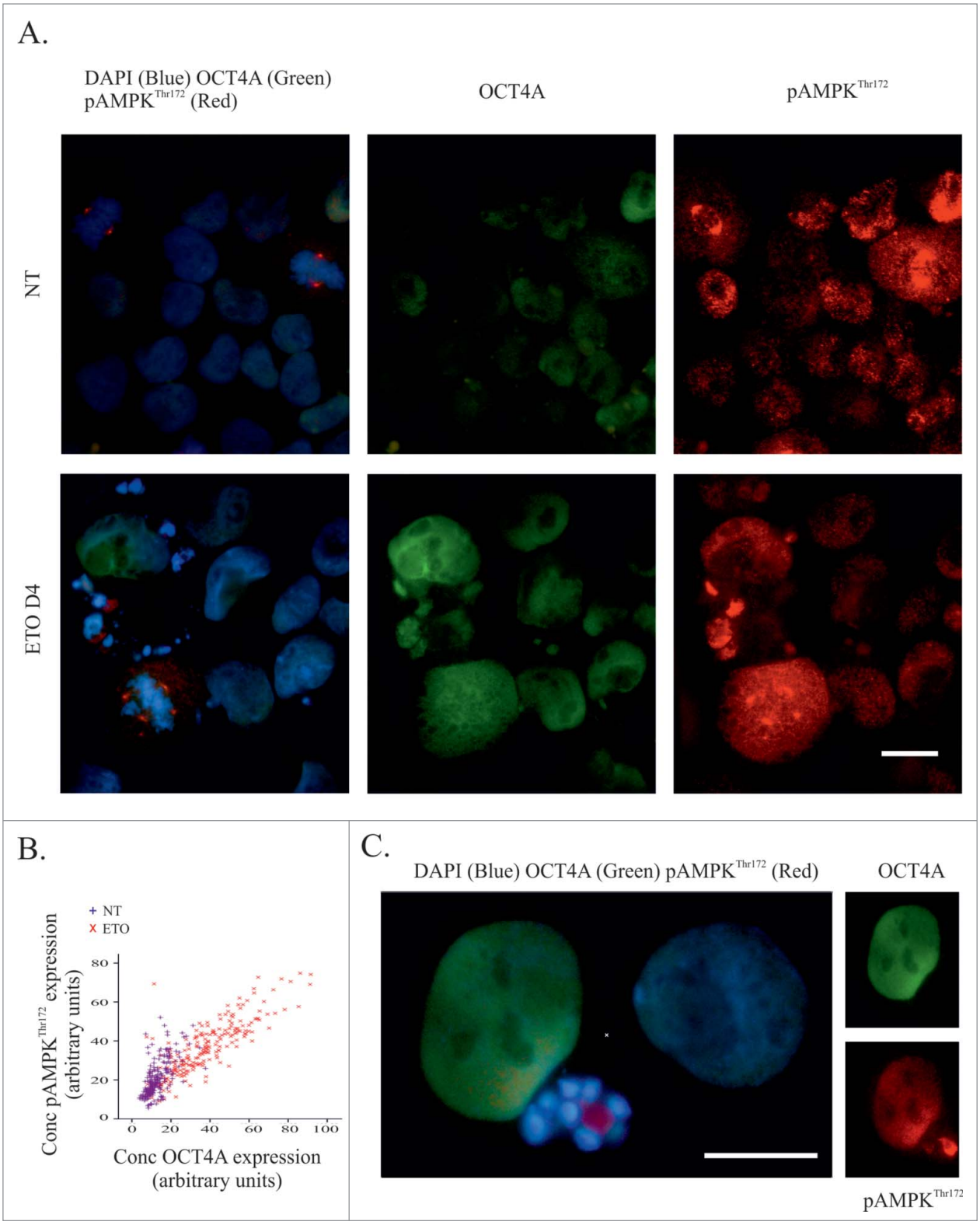

Figure 7. Activation of AMPK and OCT4A in response to ETO-treatment. PA-1 cells were treated with 8 μM ETO for 20 h and replacement with fresh media. Cells were harvested after 4 d before immunofluorescent staining for OCT4A, pAMPK^{Thr172} and DAPI. (**A**) Non-treated (upper panel) and ETO-treated (lower panel) samples were compared. AMPK and OCT4 are both activated by ETO (day 4) in interphase cells, however pAMPK is located in multiple centrosomes of arrested metaphases, while OCT4A does not; (**B**) scatterplot of image cytometry of OCT4A and pAMPK in individual cells assessed on day 4. There is a clear correlation between enhanced expression of OCT4A and pAMPK^{Thr172} of ETO-treated cells; (**C**) OCT4A and pAMPK^{Thr172} immunofluorescence in PA-1 cells 4 d after ETO-treatment. OCT4A and pAMPK^{Thr172} are mostly expressed in the same interphase nuclei, but an extremely high signal of pAMPK but not OCT4A is found within apoptotic cells. Staining of pAMPK^{Thr172} is associated with euchromatin, while the pattern of OCT4A staining is karyoplasmic (not bound to the chromatin). BRG – a 3-band optical filter. Bars =20 μm.

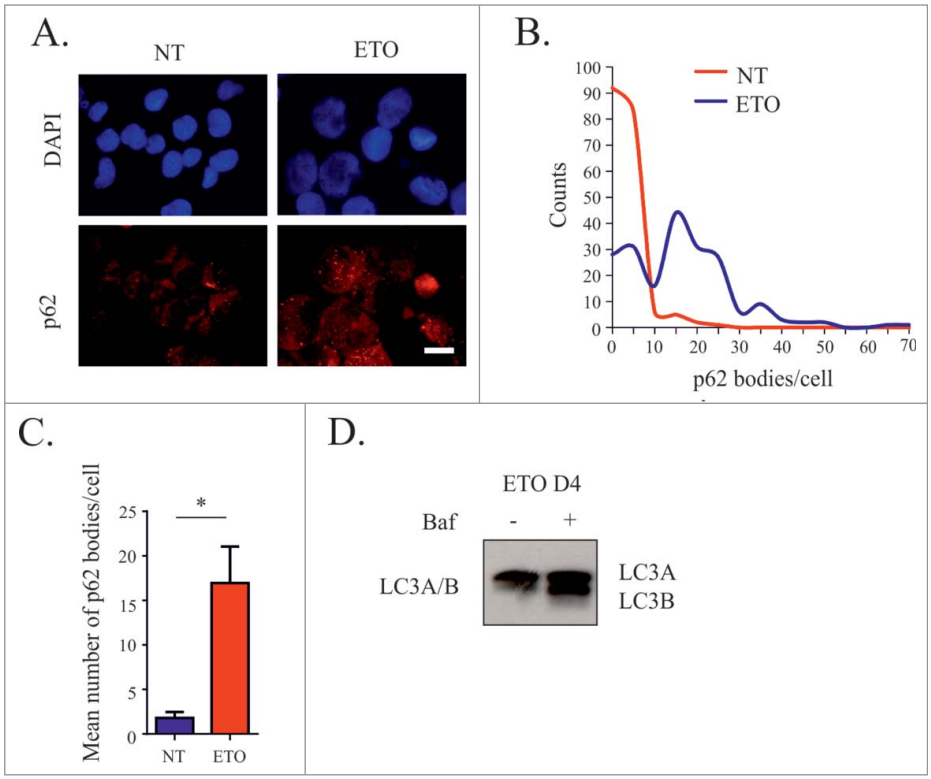

Figure 8. Assessment of macroautophagy following ETO treatment (day 4). PA-1 cells were treated with 8 μM ETO for 20 h and replacement with fresh media in the presence or absence of Baf. Cells were then stained for p62 and the number of p62 positive bodies per cell counted. (**A**) Immunofluorescent examples of staining for p62 showing foci (p62 bodies) in control and ETO-treated cells. (**B**) Representative histograms of p62 bodies/cell. (**C**) The average number of p62 bodies per cell was compared for NT and ETO treated cells from 3 independent experiments (* $p < 0.05$, $n = 3$) indicating activation by autophagy. (**D**) Immunoblotting analysis of the ratio of LC3A and LC3B with and without Baf treatment post ETO treatment. Enhanced levels of LC3B in relation to LC3A as a result of Baf treatment indicates interruption of autophagic flux in ETO treated cells. Bars = 20μm.

survival.[43] Interestingly, AMPK has also been shown to activate and stabilize p53.[44,45] Thus, the energetic stress-response of AMPK is tightly linked to the DDR of p53. The role of AMPK in the autophagy and cell death response after ETO has previously been reported.[30]

We previously revealed the p53-dependant DDR-induced elevation in OCT4A in PA-1 cells following ETO treatment. Therefore, it was not unexpected that DDR-induced OCT4A and AMPK activation should be coordinately regulated by ETO as we observed here. We found that while autophagy apparently remains functional, cells retaining both AMPK and DDR-induced OCT4A in cell nuclei are capable of preventing terminal senescence. This data are in accordance with the report by Chitikova and colleagues, [46] who demonstrated that silencing mTOR (the antagonist of AMPK suppressing autophagy) in irradiated, apoptosis-resistant cells caused a reversal of senescence. Thus OCT4A moderating p21Cip1 in collaboration with pAMPK^{Thr172}, supporting cells with metabolites and energy through autophagy and other means, channel cells through disadaptation chaos caused by high DNA damage toward a survival phenotype. ETO-treated PA-1 cells struggle against terminal senescence in particular by autophagic sequestration and removal of its regulator p16ink4a.

There is much controversy regarding markers of terminal senescence and even what the process really is. It has become recently apparent that terminal senescence is not only growth arrest,[47] moreover, it is intrinsically associated with the origin of EMT[22] and predicts poor clinical outcome after cancer treatment.[48]

In our previous and current article we have partly unravelled a mechanism showing that in response to DNA damage p53 induces 2 regulators of opposite cell fates. The setting is interesting: although they both are positively regulated by the same up-stream inducer, OCT4A suppresses p21Cip1, while the latter does not directly suppress OCT4A. Nevertheless, the scattering of the cells in expression of both through the phase space ending up in one of 2 cell fates presumes their reciprocity. The observation of cell-to-cell variability can also be a result from biological oscillations in time.[49] The best documented example of this is the p53-mdm2 oscillating system in which p53 oscillations are, indeed, crucial for cell recovery after DNA damage.[50] It is, therefore, possible that heterogeneity in p53 due to oscillations results in downstream heterogeneity of both OCT4A and p21Cip1 in PA-1 cells.

Senescence is intrinsically associated with macroautophagy induction (regulated by AMPK and persistent DNA damage). [51] Here, we found that persistent DNA damage was associated with destruction of the ternary complex of histones (H2A and H2B) and DNA in their attachment to nuclear lamin B1 using a unique antibody reagent.[32] This observation is in keeping with data of the thinning and disassembly of lamin B1 and leakage of DNA from cells as a feature of terminal senescence.[52]

Our DNA cytometric observations revealed a delay in late S-phase after ETO, augmented by BafA1. The consequence of this delay would be under-replication of heterochromatin,[53] appearance of single strand DNA breaks, demethylation and activation of the transposable elements (TE) ALU/LINE 1, whose mobility after ETO has already been described.[54] As sequestering ALU mRNA and LINE 1 by autophagy in the cytoplasm has been reported as a mechanism for protecting against transposition,[55] it therefore remains possible, (although purely speculative) that functional autophagy prevents terminal senescence in this manner also. The model with the scenario of terminal senescence

occurring due to activation of TE as discussed in several other studies.[56-58] It follows then that terminal senescence may in fact be mainly triggered by several mechanisms, which potentiate each other and result from failure of autophagy. Thus, autophagy should be a key target for preventing resistance of cancer stem cells to genotoxic therapies, a supposition supported by others.[59,60]

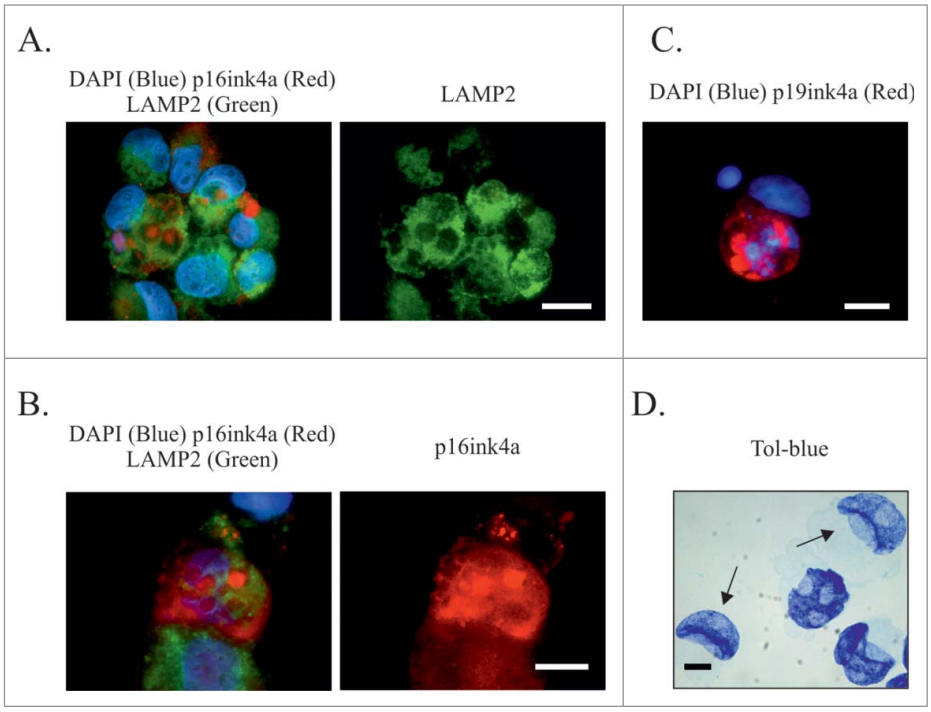

Figure 9. The relationship between autophagy functionality and senescence marker p16ink4ain ETO-treated PA-1 cells. PA-1 cells were treated with 8 μM ETO for 20 h without or with Baf, prior to media being removed and replaced with fresh media; cells were harvested 48h later (day 4). (**A, B**) imunofluorescent staining for p16ink4a (red), LAMP2 (green) or DAPI (blue). (**A**) As shown via the BRG optical filter, (**B**) only the green filter for LAMP2 demonstrating high level of functional autophagy sequestrating p16ink4a- containing aggresomes. (**B, C**) show examples of autophagic failure, where on (**B**) sequestration of p16ink4a is partly lost, diffusing in to the cytoplasm, while on (**C**) the dysfunction of autophagy is evidenced by a large vacuole overloaded with undigested p16ink4a. In all 3 cases, the nuclei are impaired: (**B**) 'laced'; (**C**) displaced and twisted by a large autophagic vacuole with some DNA lost from cell nucleus observed. These processes were observed both in ETO-treated (**B**) and more commonly in ETO+BAF(c) treated cells. (**D**) An image showing cell nuclei of normal and sickle-type shape as stained specifically for DNA with Toluidine bluein the ETO-teated specimen (sickle-like shaped nuclei are shown with arrows).

Materials and Methods

Cells

PA-1 is an ovarian teratocarcinoma (a germline tumor) cell-line, obtained from ATCC, with a stable near-diploid karyotype.[61] It possesses functional p53, in spite of possible acquisition of one mutated allele reported at passages over 407.[62] Importantly it retains the ability to differentiate into all 3 tissue types, thus possessing the features of embryonal carcinoma.[61] The NTera 2 (NT2) cell line, obtained from ATCC and used as a positive control for pluruipotency genes OCT4A, SOX2 and NANOG.

Antibodies

Primary antibodies and their uses are detailed in **Table 1**. Secondary antibodies and their uses are detailed in **Table 2**.

Cell culture and treatment

PA-1 cells were cultured in Dulbecco's modified Eagle's media (DMEM) supplemented with 10% foetal bovine serum (FBS) if not otherwise stated. NT2 cells were cultured in Dulbecco's modified Eagle's media (DMEM) supplemented with 10% foetal bovine serum (FBS). Cells were grown without antibiotics in 5% CO_2 at 37°C. Exponentially growing PA-1 cells were incubated with 4–8 μM ETO for 20 h. Following ETO treatment, cells were maintained by replenishing culture medium every 48h. Bafilomycin A (Baf A, Cayman Chemicals) 50 nM was added to the culture medium for 24h between day 3 to 4 after 20h treatment with 8 μM ETO.

Flow cytometry

Cells were harvested at relevant time points, washed in cold PBS and fixed with 70% ethanol for 20 min at room temperature. After two washes in tris buffered saline (TBS), cells were permeabilised with TBS/4% bovine serum albumin (BSA)/0.1% Triton X-100 for 10 min at room temperature. Samples were then incubated with mouse monoclonal anti-OCT4 antibody solution (Santa Cruz) and rabbit polyclonal p21Cip1 (Pierce) in TBS/4% BSA/0.1% Triton X-100 for 1h at room temperature. Following two washes in TBS, cells were incubated with goat anti-rabbit- IgG-Alexa Fluor 488 (A31627, Invitrogen) and Chicken anti-mouse IgG-Alexa Fluor 647 (A21463, Invitrogen) (1:200) in TBS/4% BSA/0.1% Triton × 100, for 30 min in the dark. DNA was counterstained with 10 μg/ml propidium iodide (PtdIns) in PBS, and assessed by flow cytometry using a FACS Aria (BD Biosciences) using Cell Quest Pro Software). Data was analyses using FlowJo analysis software.

Immunofluorescence

Cells were suspended in warm FBS and cytospun onto glass slides. Cytospins were fixed in methanol for 7 min at −20°C and dipped 10 times in ice cold acetone. Slides were then washed thrice in TBS 0.01% Tween 20 (TBST) for 5 min. Slides were subsequently blocked for 15 min in TBS, 0.05% Tween 20%, 1% BSA at room temperature. Samples were covered with TBS, 0.025% Tween 20%, 1% BSA containing primary antibody and incubated overnight at 4°C in a humidified chamber. Samples

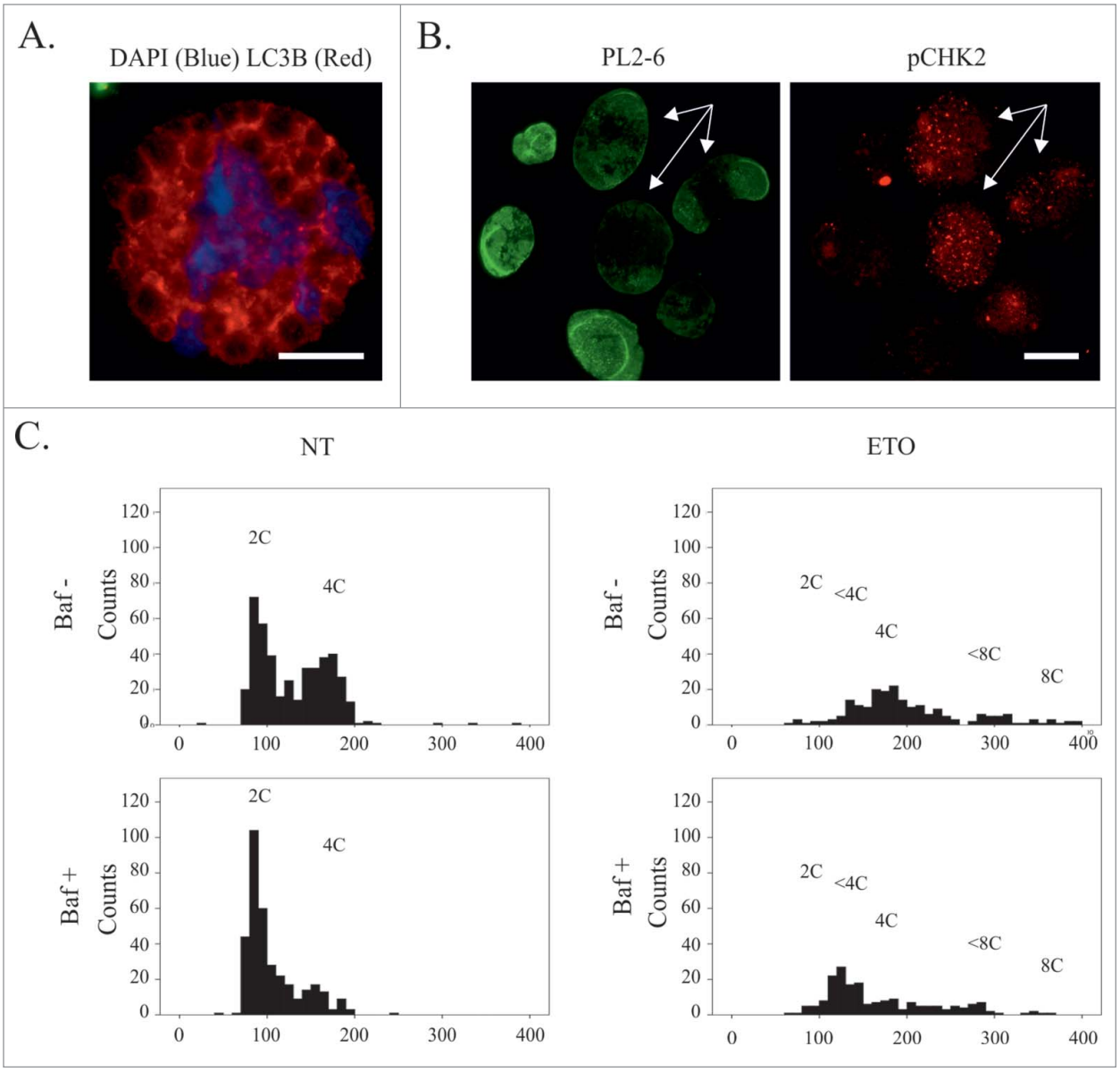

Figure 10. ETO and ETO+Baf impair cell nuclear integrity causing a delay in late S-phase in a proportion of cells with persistent DNA damage. (**A**) Disintegration of the nucleus is observed in ETO treated cells following prolonged Baf exposure (72h), where impaired autophagic flux is confirmed by alveolar structure of LC3B-positive cytoplasm in the absence of LC3 foci; Bars = 20 μm. (**B**) Persistent DNA damage leads to destruction of the epichromatin ternary complex (a specific conformation of nucleosomes attached to lamin B1) seen by a decrease in staining by the Pl2–6 antibody where Chk2-positive foci is detected in ETO-treated PA1 cells at day 4. (**C**) Representative DNA histograms obtained by image cytometry of ETO-treated and ETO+BAF-treated cells samples (day 4 after treatment); one of 3 independent experiments. BafA alone causes partial arrest in G1 in control (NT)cells and a subsequent decrease of the G2 fraction; ETO-treatment induces G2-arrest, however, a proportion of cells remain delayed in late S-phase (<4C). Cells with the DNA content <4C and 4C(G2) still reach peaks of corresponding doubling, <8C and 8C. Suppression of autophagy by Baf in ETO-treated cells favors an increase of the proportion of cells in the <4C fraction and reduces the number of cells.

were then washed thrice in TBST and covered with TBST containing the appropriate secondary antibodies (Goat anti-mouse IgG Alexa Fluor 488 (A31619, Invitrogen) and Goat anti-rabbit-IgG Alexa Fluor 594 (A31631, Invitrogen)) and incubated for 40 min at room temperature in the dark. Slides were washed thrice for 5 min with TBST and once for 2 min in PBS. Samples were then counterstained with 0.25 μg/ml DAPI for 2 min, and finally embedded in Prolong Gold (Invitrogen). When staining for p-AMPKα1/2 (alone or in combination with the antibody for OCT4), fixation in 4% paraformaldehyde for 15 min was used, followed by washing thrice in PBS 0,1% glycine. Primary antibodies and their source are listed in **Table 1**.

Microscopy and immunofluorescence image cytometry

Slides were evaluated using a Leitz Ergolux L03–10 microscope equipped with Sony DXC 390P color video camera, for

Table 1. Primary antibodies

Antibody against	Description	Specificity/immunogen	Product nr and Manufacturer	Use*
AURORA B	Rabbit polyclonal	Peptide derived from within residues 1 – 100 of Human Aurora B	ab2254, Abcam	IF
p16INK4a	Rabbit polyclonal	C-terminus of human p16	ab7962, Abcam	IF
pCHK2 (phospho T68)	Rabbit polyclonal	Epitope around the phosphorylation site of Threonine 68 (VSTpQE) of human Chk2	ab38461, Abcam	IF, W
GAPDH	Mouse monoclonal, clone 6C5	Rabbit muscle GAPDH	ab8245, Abcam	W
LAMP-2	Mouse monoclonal	The details of the immunogen for this antibody are not available.	ab25631, Abcam	IF
LC3A/B	Rabbit polyclonal	Synthetic peptide between amino acids 1–100 of the human LC3 protein	PA1–16930, Pierce	IF
LC3B	Rabbit polyclonal	Peptide derived from within residues 1 – 100 of Human LC3B	ab63817, Abcam	IF
NANOG	Mouse monoclonal, clone NNG-811	Against human Nanog.	N3038, Sigma	IF
NANOG (23D2–3C6)	Mouse monoclonal	Full-length human recombinant protein expressed in bacteria	MA-1–017, Pierce	IF
NANOG H-155	Rabbit polyclonal	epitope corresponding to amino acids 151–305 mapping at the C-terminus of Nanog of human origin	sc-33759, Santa Cruz	IF
OCT3/4	Mouse monoclonal	Peptide raised against amino acids 1–134 of Oct-3/4 of human origin non cross-reactive with Oct-3/4 isoforms B and B1	sc-5279, Santa Cruz	IF, F, W
OCT4	Rabbit polyclonal, ChIP Grade	Peptide derived from within residues 300 to the C-terminus of Human Oct4	ab19857, Abcam	IF, W
p21Cip1	Rabbit polyclonal	Raised against a peptide mapping at the C-terminusof p21 of human origin	sc-397, Santa Cruz	IF
p21Cip1	Rabbit monoclonal	Synthetic peptide corresponding to residues near the carboxy-terminus of human p21	MA5–14949, Pierce	IF, F, W
p-AMPKα1/2 (Thr183/172)	Rabbit polyclonal	Epitope corresponding to phosphorylated Thr 172 of AMPKα1 of human origin	sc-101630, Santa Cruz	IF
PL2–6	Mouse monoclonal	autoimmune anti-nucleosome antibody specifically recognizes the peripheral surface of interphase chromatin and mitotic chromosomes, epichromatin epitope	A kind gift from Olins.[32]	IF
SOX2	Mouse monoclonal	Full-length human recombinant protein expressed in bacteria	MA1–014, Pierce	IF, W
SOX2	Rabbit polyclonal	Epitope corresponding to amino acids 131–195 of Sox-2 of human origin	sc-20088x, Santa Cruz	IF
SQSTM1 (p62)	Rabbit polyclonal	Epitope corresponding to amino acids 151–440 of SQSTM1 of human origin.	sc-25575, Santa Cruz	IF

*W, western; IF, immunofluorescent staining; F, flow cytometry.

microscopic observations; in addition to separate optical filters, a 3-band BRG (blue, red, green) optical filter (Leica) was used. Image cytometry was carried out by semi-automatic measuring fluorescence values for each cell nuclei in all 3 channels and analyzed using Image-Pro Plus 4.1 software (Media Cybernetics). Apoptotic cells, determined by nuclear morphology, were omitted from measurements.

DNA image cytometry

For DNA cytometry measurements, stoichiometric toluidine blue DNA staining was performed as previously.[63] In brief, cytospins were fixed in ethanol:acetone (1:1) for >30 min at 4°C and air dried. Slides were then treated with 5N HCl for 20 min at room temperature, washed in distilled water (5 × 1 min) and stained for 10 min with 0.05% toluidine blue in

Table 2. Secondary antibodies

Antibody	Conjugate	Product No.and Manufacturer	Use*
Goat anti-mouse IgG	Alexa Fluor 488	A31619, Invitrogen	IF
Chicken anti-mouse IgG	Alexa Fluor 647	A21463, Invitrogen	F
Goat anti-rabbit- IgG	Alexa Fluor 488	A11008, Invitrogen	F
Goat anti-rabbit- IgG	Alexa Fluor 594	A31631, Invitrogen	IF
Goat anti-rabbit IgG	HRP	32460,Thermo Fisher Scientific	W
Rabbit anti-mouse IgG	HRP	61–6520, Invitrogen	W
Goat anti-rabbit IgG	IRDye 800CW	926–32211, IRDye Antibodies	W
Goat anti-mouse IgG	IRDye 800CW	926–32210, IRDye Antibodies	W
Goat anti-rabbit IgG	Goat anti-rabbit IgG	926–68021, IRDye Antibodies	W

*W, western; IF, immunofluorescent staining; F, flow cytometry.

50% citrate-phosphate McIlvain buffer pH 4. Slides were rinsed with distilled water, blotted dry and dehydrated in butanol for 2×3 min at 37°C. Samples were then incubated twice in xylene for 3 min each at room temperature and embedded in DPX (Sigma). DNA content was measured as the integral optical density with a calibrated Sony DXC 390P video camera in the green channel. Nuclear area was calculated using Image-Pro Plus 4.1 software (Media Cybernetics). Apoptotic cells were omitted from measurements. The stoichiometry of DNA staining was verified using the values obtained for metaphases compared to anaphases and telophases (ratio 2.0); the summary error of the method and device was estimated to be less than 5%.

DNA flow cytometry

Cells (including those in media) were harvested at indicated time points, washed in PBS and re-suspended in hypotonic fluorochrome solution [50 μg/ml propidium iodide (PI), 0.1% (w/v) sodium citrate, 0.1% (v/v) Triton-X-100] and stored for at least 1 h in the dark at 4°C. Flow cytometry was performed using a FACScan (BD Biosciences) or Accuri™ C6 Cytometer (BD Biosciences). Data was analyses using FlowJo analysis software.

Detection of sa-β-galactosidase activity

The senescence β-galactosidase (sa-β-gal) staining kit (Cell Signaling Technology, UK) was used to detect sa-β-gal activity in cells according to the manufacturer's protocol.

Immunoblotting

For whole-cell lysates, cells were harvested, washed once with PBS and lysed using RIPA buffer containing protease inhibitor cocktail (Sigma P8340). Protein concentrations were determined by Bradford assay (Thermo Scientific), with 10–30 μg of total protein separated on 20% SDS polyacrylamide gels followed by electrophoretic transfer onto BA85 nitrocellulose membranes (Schleicher & Schuell GmbH) overnight. Equal protein loading in each lane was confirmed by Ponceau S staining. Blots were probed with appropriate antibodies primary and secondary detected using ECL Western Blotting Substrate (Pierce™, 32106).

For comparison of OCT4 isoforms protein was transferred onto immobilon-FC transfer membrane and probed with primary antibodies. Blots were then probed with fluorescent secondary antibodies and the signal was visualized using a LICOR Odyssey imaging system.

Small interfering RNA (siRNA) silencing

FlexiTube siRNA (SI04950274, SI04950267, SI04153835 and SI00690382; Qiagen) was used to silence OCT4A expression, and FlexiTube siRNA (SI00604905, SI00604898 and SI00299810; Qiagen) was used to silence p21Cip1 expression. ON-TARGET plus non-targeting siRNA #1 (Dharmacon) was used as a negative control. Cells were transfected with siRNA using HiPerfect (Qiagen) according to the manufacturer's protocol.

Methods of statistical analysis

Statistical analysis was performed in GraphPad (GraphPad Software Ltd). Student t-test was used to calculate the statistical significance of difference of means where appropriate. Statistical significance was accepted when $p < 0.05$. Graphs were plotted in GraphPad Prism 5 and IBM SPSS statistics 22.

Disclosure of Potential Conflicts of Interest

No potential conflicts of interest were disclosed.

Acknowledgments

The authors would like to thank Professor Hao and Dr Zhao, Dept of Histology and Embryology, Shandong University School of Medicine for the kind gift of the OCT4A and OCT4A-Psg-1 vector constructs and Ada and Donald Olins for providing the antibody for epichromatin.

Funding

The project was funded through an MRC PhD studentship and the Gerald Kerkut Charitable Trust, the University of Manchester Project Diamond and the Manchester Cancer Research Center and by the Europe Social Fund Project, project No.

2013/0023/1DP/1.1.1.2.0/13/APIA/VIAA/037. The publishing costs associated with this article are in part provided by the Manchester Project Diamond and by the Europe Social Fund Project, project No. 2013/0023/1DP/1.1.1.2.0/13/APIA/VIAA/037.

Supplemental Material

Supplemental data for this article can be accessed on the publisher's website.

References

1. Ben-Porath I, Thomson MW, Carey VJ, Ge R, Bell GW, Regev A, Weinberg RA. An embryonic stem cell-like gene expression signature in poorly differentiated aggressive human tumors. Nat Genet 2008; 40(5): 499-507; PMID:18443585; http://dx.doi.org/10.1038/ng.127
2. Reya T, Morrison SJ, Clarke MF, Weissman IL. Stem cells, cancer, and cancer stem cells. Nature 2001; 414 (6859): 105-111; PMID:11689955; http://dx.doi.org/10.1038/35102167
3. Chiou SH, Yu CC, Huang CY, Lin SC, Liu CJ, Tsai TH, Chou SH, Chien CS, Ku HH, Lo JF. Positive correlations of Oct-4 and Nanog in oral cancer stem-like cells and high-grade oral squamous cell carcinoma. Clin Cancer Res 2008; 14(13): 4085-4095; PMID:18593985; http://dx.doi.org/10.1158/1078-0432.CCR-07-4404
4. Meng HM, Zheng P, Wang XY, Liu C, Sui HM, Wu SJ, Zhou J, Ding YQ, Li JM. Overexpression of nanog predicts tumor progression and poor prognosis in colorectal cancer. Cancer Biol Ther 2010; 9(4): 295-302; PMID:20026903; http://dx.doi.org/10.4161/cbt.9.4.10666
5. Du LT, Yang YM, Xiao XY, Wang CX, Zhang XH, Wang LL, Zhang X, Li W, Zheng GX, Wang S. others. Sox2 nuclear expression is closely associated with poor prognosis in patients with histologically node-negative oral tongue squamous cell carcinoma. Oral Oncol 2011; 47(8): 709-713; PMID:21689966; http://dx.doi.org/10.1016/j.oraloncology.2011.05.017
6. Lengerke C, Fehm T, Kurth R, Neubauer H, Scheble V, Muller F, Schneider F, Petersen K, Wallwiener D, Kanz L. others. Expression of the embryonic stem cell marker SOX2 in early-stage breast carcinoma. Bmc Cancer 2011; 11:42; PMID:21276239; http://dx.doi.org/10.1186/1471-2407-11-42
7. He W, Li K, Wang F, Qin YR, Fan QX. Expression of OCT4 in human esophageal squamous cell carcinoma is significantly associated with poorer prognosis. World J Gastroenterol 2012; 18(7): 712-719; PMID:22363145; http://dx.doi.org/10.3748/wjg.v18.i7.712
8. Huang P, Chen J, Wang L, Na YQ, Kaku H, Ueki H, Sasaki K, Yamaguchi K, Zhang K, Saika T. others. Implications of transcriptional factor, OCT-4, in human bladder malignancy and tumor recurrence. Med Oncol 2012; 29(2): 829-834; PMID:21533858; http://dx.doi.org/10.1007/s12032-011-9962-4
9. Lin T, Ding YQ, Li JM. Overexpression of Nanog protein is associated with poor prognosis in gastric adenocarcinoma. Med Oncol 2012; 29(2): 878-885; PMID:21336986; http://dx.doi.org/10.1007/s12032-011-9860-9
10. Lagadec C, Vlashi E, Della Donna L, Dekmezian C, Pajonk F. Radiation-Induced Reprogramming of Breast Cancer Cells. Stem Cells 2012; 30(5): 833-844; PMID:22489015; http://dx.doi.org/10.1002/stem.1058
11. Abubaker K, Latifi A, Luwor R, Nazaretian S, Zhu HJ, Quinn MA, Thompson EW, Findlay JK, Ahmed N. Short-term single treatment of chemotherapy results in the enrichment of ovarian cancer stem cell-like cells leading to an increased tumor burden. Mol Cancer 2013; 12; PMID:23537295; http://dx.doi.org/10.1186/1476-4598-12-24
12. Salmina K, Jankevics E, Huna A, Perminov D, Radovica I, Klymenko T, Ivanov A, Jascenko E, Scherthan H, Cragg M. others. Up-regulation of the embryonic self-renewal network through reversible polyploidy in irradiated p53-mutant tumour cells. Exp Cell Res 2010; 316(13): 2099-2112
13. Roninson IB. Tumor cell senescence in cancer treatment. Cancer Res 2003; 63(11): 2705-2715; PMID:12782571
14. Roninson IB, Broude EV, Chang BD. If not apoptosis, then what? - Treatment-induced senescence and mitotic catastrophe in tumor cells. Drug Resistance Updates 2001; 4(5): 303-313; PMID:11991684; http://dx.doi.org/10.1054/drup.2001.0213
15. Sherman MY, Meng L, Stampfer M, Gabai VL, Yaglom JA. Oncogenes induce senescence with incomplete growth arrest and suppress the DNA damage response in immortalized cells. Aging Cell 2011; 10(6): 949-961; PMID:21824272; http://dx.doi.org/10.1111/j.1474-9726.2011.00736.x
16. Puig PE, Guilly MN, Bouchot A, Droin N, Cathelin D, Bouyer F, Favier L, Ghiringhelli F, Kroemer G, Solary E. others. Tumor cells can escape DNA-damaging cisplatin through DNA endoreduplication and reversible polyploidy. Cell Biol Int 2008; 32(9): 1031-1043.
17. Roberson RS, Kussick SJ, Vallieres E, Chen SYJ, Wu DY. Escape from therapy-induced accelerated cellular senescence in p53-null lung cancer cells and in human lung cancers. Cancer Res 2005; 65(7): 2795-2803; PMID:15805280; http://dx.doi.org/10.1158/0008-5472.CAN-04-1270
18. Sabisz M. Skladanowski A. Cancer stem cells and escape from drug-induced premature senescence in human lung tumor cells Implications for drug resistance and in vitro drug screening models. Cell Cycle 2009; 8(19): 3208-3217; PMID:19738435; http://dx.doi.org/10.4161/cc.8.19.9758
19. Banito A, Rashid ST, Acosta JC, Li S, Pereira CF, Geti I, Pinho S, Silva JC, Azuara V, Walsh M. others. Senescence impairs successful reprogramming to pluripotent stem cells. Genes Dev 2009; 23(18): 2134-2139; PMID:19696146; http://dx.doi.org/10.1101/gad.1811609
20. Jaenisch R. Nuclear cloning and direct reprogramming: the long and the short path to Stockholm. Cell Stem Cell 2012; 11(6): 744-747; PMID:23217419; http://dx.doi.org/10.1016/j.stem.2012.11.005
21. Storer M, Mas A, Robert-Moreno A, Pecoraro M, Ortells MC, Di Giacomo V, Yosef R, Pilpel N, Krizhanovsky V, Sharpe J. others. Senescence is a developmental mechanism that contributes to embryonic growth and patterning. Cell 2013; 155(5): 1119-1130; PMID:24238961; http://dx.doi.org/10.1016/j.cell.2013.10.041
22. Kishi S, Bayliss PE, Hanai JI. A prospective epigenetic paradigm between cellular senescence and epithelial-mesenchymal transition in organismal development and aging. Transl Res 2015; 165(1): 241-249; PMID:24924348; http://dx.doi.org/10.1016/j.trsl.2014.05.007
23. Huna A, Salmina K, Jascenko E, Duburs G, Inashkina I, Erenpreisa J. Self-Renewal Signalling in Presenescent Tetraploid IMR90 Cells. J Aging Res 2011; 2011: 103253; PMID:21629737; http://dx.doi.org/10.4061/2011/103253
24. Jackson TR, Salmina K, Huna A, Inashkina I, Jankevics E, Riekstina U, Kalnina Z, Ivanov A, Townsend PA, Cragg MS. others. DNA damage causes TP53-dependent coupling of self-renewal and senescence pathways in embryonal carcinoma cells. Cell Cycle 2013; 12(3): 430-441; PMID:23287532; http://dx.doi.org/10.4161/cc.23285
25. Boyer LA, Lee TI, Cole MF, Johnstone SE, Levine SS, Zucker JR, Guenther MG, Kumar RM, Murray HL, Jenner RG. others. Core transcriptional regulatory circuitry in human embryonic stem cells. Cell 2005; 122 (6): 947-956; PMID:16153702; http://dx.doi.org/10.1016/j.cell.2005.08.020
26. Marques-Torrejon MA, Porlan E, Banito A, Gomez-Ibarlucea E, Lopez-Contreras AJ, Fernandez-Capetillo O, Vidal A, Gil J, Torres J, Farinas I. Cyclin-Dependent Kinase Inhibitor p21 Controls Adult Neural Stem Cell Expansion by Regulating Sox2 Gene Expression. Cell Stem Cell 2013; 12(1): 88-100; PMID:23260487; http://dx.doi.org/10.1016/j.stem.2012.12.001
27. Sun Y, Connors KE, Yang DQ. AICAR induces phosphorylation of AMPK in an ATM-dependent, LKB1-independent manner. Mol Cell Biochem 2007; 306(1-2): 239-245; PMID:17786544; http://dx.doi.org/10.1007/s11010-007-9575-6
28. Vazquez-Martin A, Lopez-Bonet E, Oliveras-Ferraros C, Perez-Martinez MC, Bernado L, Menendez JA. Mitotic kinase dynamics of the active form of AMPK (phospho-AMPK α(Thr172)) in human cancer cells. Cell Cycle 2009; 8(5): 788-791; PMID:19221486; http://dx.doi.org/10.4161/cc.8.5.7787
29. Kim J, Kundu M, Viollet B, Guan KL. AMPK and mTOR regulate autophagy through direct phosphorylation of Ulk1. Nat Cell Biol 2011; 13(2): 132-U71; PMID:21258367; http://dx.doi.org/10.1038/ncb2152
30. Xie BS, Zhao HC, Yao SK, Zhuo DX, Jin B, Lv DC, Wu CL, Ma DL, Gao C, Shu XM. others. Autophagy inhibition enhances etoposide-induced cell death in human hepatoma G2 cells. Int J Mol Med 2011; 27 (4): 599-606; PMID:21274505
31. Rayess H, Wang MB, Srivatsan ES. Cellular senescence and tumor suppressor gene p16. Int J Cancer 2012; 130(8): 1715-1725; http://dx.doi.org/10.1002/ijc.27316
32. Olins AL, Langhans M, Monestier M, Schlotterer A, Robinson DG, Viotti C, Zentgraf H, Zwerger M, Olins DE. An epichromatin epitope Persistence in the cell cycle and conservation in evolution. Nucleus-Austin 2011; 2(1): 47-60; http://dx.doi.org/10.4161/nucl.13655
33. Lee J, Go Y, Kang I, Han YM, Kim J. Oct-4 controls cell-cycle progression of embryonic stem cells. Biochem J 2010; 426: 171-181; PMID:19968627; http://dx.doi.org/10.1042/BJ20091439
34. Bartova E, Sustackova G, Stixova L, Kozubek S, Legartova S, Foltankova V. Recruitment of Oct4 Protein to UV-Damaged Chromatin in Embryonic Stem Cells. Plos One 2011; 6(12); PMID:22164208; http://dx.doi.org/10.1371/journal.pone.0027281
35. Gorban AN, Smirnova EV, Tyukina TA. Correlations, risk and crisis: From physiology to finance. Physica A-Statistical Mechanics Its Applications 2010; 389(16): 3193-3217: http://dx.doi.org/10.1016/j.physa.2010.03.035
36. Stuart A. Kauffman, "The origins of order: Self-organization and selection in evolution.,"in (Oxford university press, 2013)
37. Huang S. Non-genetic heterogeneity of cells in development: more than just noise. Development 2009; 136 (23): 3853-3862; PMID:19906852; http://dx.doi.org/10.1242/dev.035139
38. Edgar BA, Orr-Weaver TL. Endoreplication cell cycles: More for less. Cell 2001; 105(3): 297-306; PMID:11348589; http://dx.doi.org/10.1016/S0092-8674(01)00334-8
39. Kalmar T, Lim C, Hayward P, Munoz-Descalzo S, Nichols J, Garcia-Ojalvo J, Arias AM. Regulated Fluctuations in Nanog Expression Mediate Cell Fate Decisions in Embryonic Stem Cells. Plos Biol 2009; 7(7); PMID:19582141; http://dx.doi.org/10.1371/journal.pbio.1000149
40. Lin TX, Chao C, Saito S, Mazur SJ, Murphy ME, Appella E, Xu Y. P53 induces differentiation of mouse embryonic stem cells by suppressing Nanog expression.

Nat Cell Biol 2005; 7(2): 165-U80; PMID:15619621; http://dx.doi.org/10.1038/ncb1211
41. Sanli T, Steinberg GR, Singh G, Tsakiridis T. AMP-activated protein kinase (AMPK) beyond metabolism A novel genomic stress sensor participating in the DNA damage response pathway. Cancer Biol Ther 2014; 15 (2): 156-169; PMID:24100703; http://dx.doi.org/10.4161/cbt.26726
42. Vazquez-Martin A, Oliveras-Ferraros C, Cufi S, Martin-Castillo B, Menendez JA. Metformin activates an Ataxia Telangiectasia Mutated (ATM)/Chk2-regulated DNA damage-like response. Cell Cycle 2011; 10(9): 1499-1501; PMID:21566461; http://dx.doi.org/10.4161/cc.10.9.15423
43. Bungard D, Fuerth BJ, Zeng PY, Faubert B, Maas NL, Viollet B, Carling D, Thompson CB, Jones RG, Berger SL. Signaling Kinase AMPK Activates Stress-Promoted Transcription via Histone H2B Phosphorylation. Science 2010; 329(5996): 1201-1205; PMID:20647423; http://dx.doi.org/10.1126/science.1191241
44. Jones RG, Plas DR, Kubek S, Buzzai M, Mu J, Xu Y, Birnbaum MJ, Thompson CB. AMP-activated protein kinase induces a p53-dependent metabolic checkpoint. Mol Cell 2005; 18(3): 283-293; PMID:15866171; http://dx.doi.org/10.1016/j.molcel.2005.03.027
45. Lee CW, Wong LLY, Tse EYT, Liu HF, Leong VYL, Lee JMF, Hardie DG, Ng IOL, Ching YP. AMPK Promotes p53 Acetylation via Phosphorylation and Inactivation of SIRT1 in Liver Cancer Cells. Cancer Res 2012; 72(17): 4394-4404; PMID:22728651; http://dx.doi.org/10.1158/0008-5472.CAN-12-0429
46. Chitikova ZV, Gordeev SA, Bykova TV, Zubova SG, Pospelov VA, Pospelova TV. Sustained activation of DNA damage response in irradiated apoptosis-resistant cells induces reversible senescence associated with mTOR downregulation and expression of stem cell markers. Cell Cycle 2014; 13(9): 1424-1439; PMID:24626185; http://dx.doi.org/10.4161/cc.28402
47. Blagosklonny MV. Cell cycle arrest is not senescence. Aging-Us 2011; 3(2): 94-101.
48. Wang Q, Wu PC, Dong DZ, Ivanova I, Chu E, Zeliadt S, Vesselle H, Wu DY. Polyploidy road to therapy-induced cellular senescence and escape. Int J Cancer 2013; 132(7): 1505-1515; http://dx.doi.org/10.1002/ijc.27810
49. Brock A, Chang H, Huang S. OPINION Non-genetic heterogeneity - a mutation-independent driving force for the somatic evolution of tumours. Nat Rev Genet 2009; 10(5): 336-342; PMID:19337290; http://dx.doi.org/10.1038/nrg2556
50. Purvis JE, Karhohs KW, Mock C, Batchelor E, Loewer A, Lahav G. p53 Dynamics Control Cell Fate. Science 2012; 336(6087): 1440-1444; PMID:22700930; http://dx.doi.org/10.1126/science.1218351
51. Capparelli C, Chiavarina B, Whitaker-Menezes D, Pestell TG, Pestell RG, Hulit J, Ando S, Howell A, Martinez-Outschoorn UE, Sotgia F, others. CDK inhibitors (p16/p19/p21) induce senescence and autophagy in cancer-associated fibroblasts, "fueling" tumor growth via paracrine interactions, without an increase in neo-angiogenesis. Cell Cycle 2012; 11(19): 3599-3610; PMID:22935696; http://dx.doi.org/10.4161/cc.21884
52. Ivanov A, Pawlikowski J, Manoharan I, van Tuyn J, Nelson DM, Rai TS, Shah PP, Hewitt G, Korolchuk VI, Passos JF, others. Lysosome-mediated processing of chromatin in senescence. J Cell Biol. 2013; 202(1): 129-143; PMID:23816621; http://dx.doi.org/10.1083/jcb.201212110
53. Nagl Walter. Endopolyploidy and polyteny in differentiation and evolution. 1978
54. Hagan CR, Sheffield RF, Rudin CM. Human Alu element retrotransposition induced by genotoxic stress. Nat Genet 2003; 35(3): 219-220; PMID:14578886; http://dx.doi.org/10.1038/ng1259
55. Guo HS, Chitiprolu M, Gagnon D, Meng LR, Perez-Iratxeta C, Lagace D, Gibbings D. Autophagy supports genomic stability by degrading retrotransposon RNA. Nat Commun 2014; 5:5276
56. Wang JR, Geesman GJ, Hostikka SL, Atallah M, Blackwell B, Lee E, Cook PJ, Pasaniuc B, Shariat G, Halperin E, others. Inhibition of activated pericentromeric SINE/Alu repeat transcription in senescent human adult stem cells reinstates self-renewal. Cell Cycle 2011; 10(17): 3016-3030; PMID:21862875; http://dx.doi.org/10.4161/cc.10.17.17543
57. Baker DJ, Sedivy JM. Probing the depths of cellular senescence. J Cell Biol 2013; 202(1): 11-13; PMID:23816622; http://dx.doi.org/10.1083/jcb.201305155
58. Cecco M, Criscione SW, Peckham EJ, Hillenmeyer S, Hamm EA, Manivannan J, Peterson AL, Kreiling JA, Neretti N, Sedivy JM. Genomes of replicatively senescent cells undergo global epigenetic changes leading to gene silencing and activation of transposable elements. Aging Cell 2013; 12(2): 247-256; PMID:23360310; http://dx.doi.org/10.1111/acel.12047
59. Sui X, Chen R, Wang Z, Huang Z, Kong N, Zhang M, Han W, Lou F, Yang J, Zhang Q, others. Autophagy and chemotherapy resistance: a promising therapeutic target for cancer treatment. Cell Death Dis 2013; 4: e838
60. Dorr JR, Yu Y, Milanovic M, Beuster G, Zasada C, Dabritz JHM, Lisec J, Lenze D, Gerhardt A, Schleicher K, others. Synthetic lethal metabolic targeting of cellular senescence in cancer therapy. Nature 2013; 501 (7467):421-5; PMID:23945590; http://dx.doi.org/10.1038/nature12437
61. Zeuthen J, Norgaard JOR, Avner P, Fellous M, Wartiovaara J, Vaheri A, Rosen A, Giovanella BC. Characterization of A Human Ovarian Teratocarcinoma-Derived Cell-Line. Int J Cancer 1980; 25(1): 19-32; http://dx.doi.org/10.1002/ijc.2910250104
62. Gao C, Miyazaki M, Li JW, Tsuji T, Inoue Y, Namba M. Cytogenetic characteristics and p53 gene status of human teratocarcinoma PA-1 cells in 407–445 passages. Int J Mol Med 1999; 4(6): 597-600; PMID:10567668
63. Erenpreisa J, Freivalds T. Anisotropic staining of apurinic acid with toluidine blue. Histochemistry 1979; 60 (3): 321-325; PMID:89109; http://dx.doi.org/10.1007/BF00500660